Applied Physics Letters

RESEARCH ARTICLE | JUNE 24 2025

Quantum dots solar cells under mimic high altitude platform satellites environments

Ram Datt ; Xin Wen ; Xiaobo Ding ; Zeke Liu ; Wanli Ma ; Wing Chung Tsoi

Appl. Phys. Lett. 126, 253904 (2025)
https://doi.org/10.1063/5.0278791

AIP Publishing

Applied Physics Letters ARTICLE pubs.aip.org/aip/apl

Quantum dots solar cells under mimic high altitude platform satellites environments

Cite as: Appl. Phys. Lett. **126**, 253904 (2025); doi: 10.1063/5.0278791
Submitted: 2 May 2025 · Accepted: 7 June 2025 ·
Published Online: 24 June 2025

View Online Export Citation CrossMark

Ram Datt,[1] Xin Wen,[2] Xiaobo Ding,[2] Zeke Liu,[2,3,a)] Wanli Ma,[2,3] and Wing Chung Tsoi[1,a)]

AFFILIATIONS

[1]SPECIFIC, Faculty of Science and Engineering, Swansea University, Bay Campus, Fabian Way, Swansea SA1 8EN, United Kingdom
[2]Institute of Functional Nano & Soft Materials (FUNSOM), Joint International Research Laboratory of Carbon-Based Functional Materials and Devices, Soochow University, Suzhou 215123, Jiangsu, People's Republic of China
[3]Jiangsu Key Laboratory of Advanced Negative Carbon Technologies, Soochow University, Suzhou 215123, Jiangsu, People's Republic of China

[a)]**Authors to whom correspondence should be addressed:** zkliu@suda.edu.cn and w.c.tsoi@swansea.ac.uk

ABSTRACT

Quantum dot solar cells are solution-processable, lightweight, and low-cost, and their long-term stability makes them attractive to explore for aerospace applications. In this work, we have studied lead sulfide (PbS) colloidal quantum dot solar cells (CQDSCs) using three different types of hole transport layer combinations, such as PbS-MPA/PbS-MPA (PbS-MPA), P3HT/PTAA (P3HT), and PBDB-T/MoO_3(PBDB-T), under mimic working environmental conditions for high altitude platform satellites (HAPS). It includes ultraviolet rich solar irradiation (AM0), low temperature conditions (+10 to −20 °C), and low pressure. The thermal cycling (considering change in temperature at day–night) measurements were also conducted. The device performance under a broad range of temperatures from +80 to −100 °C was also included. The devices delivered power conversion efficiency (PCE) of 9.46 (8.41), 9.68 (7.86), and 11.77 (10.75)% for PbS-MPA, P3HT, and PBDB-T devices under AM1.5G(AM0), respectively. PbS-MPA devices maintain the PCE and slightly improve their performance under low temperatures (from 0 down to −100 °C). Meanwhile, the P3HT and PBDB-T-based CQDSCs devices started to decline in PCE significantly from −40 and +10 °C, respectively. Furthermore, PbS-MPA devices show excellent thermal cycling stability, making them attractive for further exploration for aerospace applications.

Quantum dots, a nanometer-sized diameter materials, have been used as an active element in a wide range of applications such as field effect transistor, solar cells, photodetectors, and light-emitting diodes.[1–6] Lead sulfide (PbS) quantum dot's absorption in visible and near-infrared, bandgap tunability, and solution processability make them attractive for solar cells applications.[7–12] Recent developments in device structure and passivation of interfaces in PbS colloidal quantum dots solar cells (CQDSCs) delivered the record high power conversion efficiency (PCE) up to 15.45% under AM1.5G.[13] Furthermore, the low cost and compatibility with flexible substrate made them a potential candidate for aerospace applications. High altitude platform satellites (HAPS) (also known as high altitude pseudo-satellite or high altitude platform station) are a place between 20 and 25 km (from earth surface) in stratosphere and could be used for flying unmanned aerial vehicles (UAV) and high-altitude balloons (HAB) for different purposes including defense, natural disaster relief and monitoring, and disaster recovery communication.[14,15] With the help of solar cells, the UAV and HAB can operate for the longer period of time without worrying about power supply and CQDSCs could be applied under HAPS regions. The environment under HAPS includes AM0 (136.6 mW/cm^2) irradiation, variation in temperature (+10 to −20 °C in daytime and could go up to −85 °C in night), and low pressure (1–250 mbar).[16] Due to high cost and low specific power of inorganic solar cells, researchers are exploring other options and CQDSCs could be an alternative. Tavakoli *et al.* demonstrated flexible substrate based PbS quantum dots solar cells and delivered PCE of 7.1%; remarkably, the device showed specific power (power-per-weight) of 12.3 W/g. Furthermore, PbS CQDSCs using silver nanowire-based electrode on a

flexible substrate have delivered specific power up to 15.2 W/g (expected to improve near future), which is much higher than the existing inorganic solar cells (Si—0.38 W/g and multijunction—3.8 W/g).[17–19] Speirs *et al.* explored the temperature dependent behavior of PbS quantum dots solar cells in the range of 295 to 180 K and received maximum PCE at 230 K, which suggested the working ability of PbS quantum dots solar cells under low temperatures.[20] High specific power and high low temperature performance motive us to study CQDSCs for HAPS applications. In this work, we have included PbS colloidal quantum dots based on three types (changing different hole transport layer combinations) of CQDSCs, studied them under a HAPS environment, and included thermal cycling stability.

The material details and device fabrication procedures are summarized in the supplementary material (Sec. S1). For the simplicity, the device structure in Figs. 1(a)–1(c) is named as PbS-MPA [PbS functionalized with 3-mercaptopropionic acid (MPA)], P3HT, and PBDB-T, respectively, throughout the manuscript, based on using the combination of hole transport layers. The current density–voltage (J-V) measurement was conducted under AM1.5G and AM0 using the Newport solar simulator (model no. 94023A). External quantum efficiency (EQE) measurement has been completed using inhouse EQE setup at 71 Hz chopping frequency. A Linkam Scientific system is used to mimic HAPS environment, and the liquid nitrogen was used to get low temperature. The chamber pressure was maintained at 10 mbar.

The photovoltaic performance of PbS-MPA, P3HT, and PBDB-T CQDSCs devices was examined under AM1.5G (100 mW/cm^2) testing conditions using a class AAA solar simulator, and the light intensity was calibrated by a standard silicon cell. For the AM0 (136.6 mW/cm^2) irradiation, the AM1.5G filter was replaced with an AM0 filter and the light intensity was calibrated using the integrated current density (J_{EQE}) values, calculated for CQDSCs devices using the AM0 spectrum. Figures 2(a)–2(c) show the J-V characteristics measured under AM1.5G and AM0 at room temperature. The PbS-MPA, P3HT, and PBDB-T CQDSCs devices showed PCE under AM 1.5G of 9.46%, 9.68%, and 11.77%, respectively. Meanwhile, the corresponding PCE under AM0 was 8.41%, 7.86%, and 10.75%, respectively. The main changes can be seen in short-circuit current density (J_{SC}), whereas open-circuit voltage (V_{OC}) and fill factor (FF) were similar under AM1.5G and AM0. J_{SC} under AM1.5G (AM0) was 27.92 (34.90), 27.05(30.01), and 26.71 (33.01) mA/cm^2 of PbS-MPA, P3HT, and PBDB-T CQDSCs devices, respectively. The difference between J_{SC} and J_{EQE} was under 5% for both AM1.5G and AM0 irradiations, as the EQE graphs are shown in Figs. 2(d)–2(f). The drop in PCE under AM0 is due to a change in the light spectrum. Table I summarizes the photovoltaic parameters of the PbS-MPA, P3HT, and PBDB-T CQDSCs. The PbS-MPA and PBDB-T CQDSCs devices PCE under AM0 were ∼0.90 of AM1.5G, which is higher than P3HT's PCE (∼0.81xAM1.5G). It is due to high EQE [Fig. 1(d)] in the AM0 irradiation region for PbS-MPA and PBDB-T CQDSCs. P3HT devices show a bit of hysteresis while measuring them in forward and revers scan (Fig. S1 in the supplementary material) compared to PbS-MPA and PBDB-T CQDSCs under AM 1.5G and AM0 irradiation.

The temperature range for the CQDSCs devices measurement was considered as per the HAPS environment, varying from +10 to −20 °C in the daytime. In addition, a broad range of temperatures, from +80 to −100 °C, has also been included to explore the possibility of CQDSCs devices beyond HAPS applications. The J-V characteristics of devices measured at different temperatures are shown in Fig. S2 (supplementary material). Figure 3 shows the normalized device parameters measured under different temperatures for PbS-MPA, P3HT, and PBDB-T CQDSCs devices, and their individual devices normalized parameters are shown in Fig. S3 (supplementary material). V_{OC} [Fig. 3(a)] improved as the temperature went down from +20 to −100 °C, and the improvement was similar for PbS-MPA and P3HT devices, whereas V_{OC} improvement in the PBDB-T device was more pronounced. V_{OC} of PbS-MPA devices had a higher decline at high temperatures (80 °C) compared to P3HT and PBDB-T devices. Figure 3(b) shows the change in J_{SC} under different temperature ranges; for PbS-MPA devices, there was no decline in J_{SC} over low and high temperatures. At the same time, J_{SC} of P3HT devices declined slightly after −90 °C, while decline was more pronounced at high temperatures (+60 and +80 °C). The PBDB-T devices showed a decline in J_{SC} even below 0 °C and dropped up to 25% at −100 °C. Figure 3(c) shows the change in FF, and PbS-MPA devices retained 100% values down to −50 °C and only 10% (compared to the value measured at +20 °C) declined at −100 °C. However, for P3HT and PBDB-T, the decline in FF even started at −40 and 0 °C, respectively. At −100 °C, P3HT and PBDB-T CQDSCs devices FF dropped up to 20% and 35%,

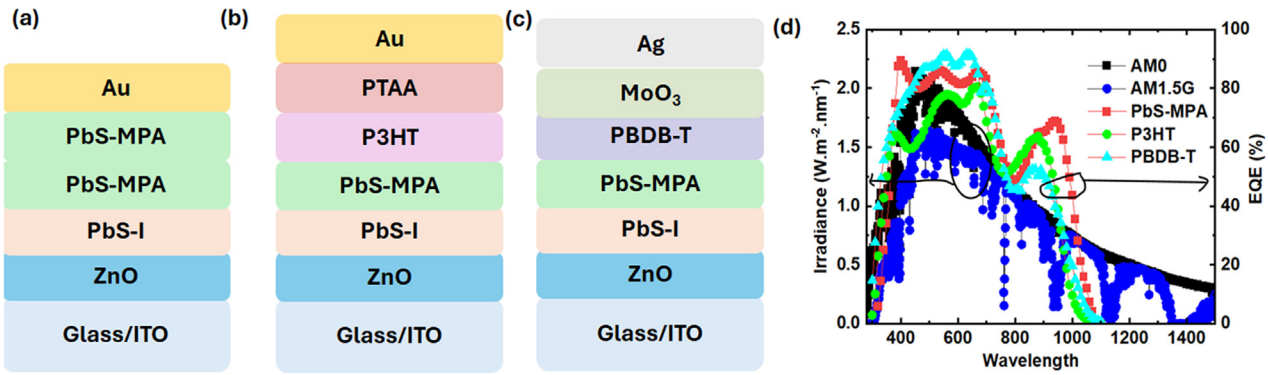

FIG. 1. Device structures of (a) PbS-MPA, (b) P3HT, and (c) PBDB-T based CQDSCs. (d) EQE (of PbS-MPA, P3HT, and PBDB-T devices) and solar spectrum of AM1.5G and AM0 irradiation.

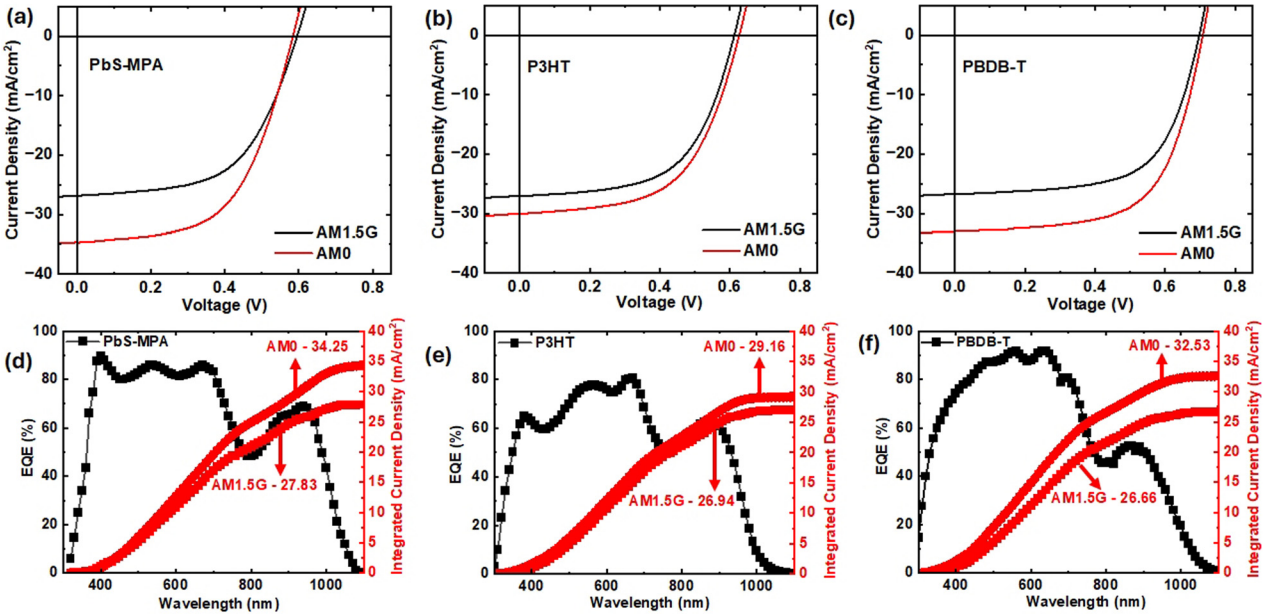

FIG. 2. J-V characteristics measured (forward scan) under AM1.5G and AM0 of (a) PbS-MPA, (b) P3HT, and (c) PBDB-T CQDSCs devices. EQE spectra's (including calculated integrated current density) of (d) PbS-MPA, (e) P3HT, and (f) PBDB-T CQDSCs devices.

TABLE I. The PbS-MPA, P3HT, and PBDB-T CQDSCs devices summary, measured under AM1.5G and AM0 irradiation.

Devices	Irradiation	Scan	V_{OC} (V)	J_{SC}(mA/cm^2)	J_{EQE} (mA/cm^2)	FF (%)	PCE (%)
PbS-MPA	AM1.5G	Forward	0.595	27.92	27.83	57.05	9.46
		Reverse	0.586	27.68		55.52	9.00
	AM0	Forward	0.583	34.90	34.25	56.55	8.41
		Reverse	0.573	34.86		55.22	8.07
P3HT	AM1.5G	Forward	0.611	27.05	26.94	58.50	9.68
		Reverse	0.605	26.32		54.21	8.64
	AM0	Forward	0.626	30.01	29.16	57.25	7.86
		Reverse	0.618	30.19		54.71	7.46
PBDB-T	AM1.5G	Forward	0.696	26.73	26.66	63.33	11.7
		Reverse	0.691	26.59		62.15	11.4
	AM0	Forward	0.707	33.01	32.53	62.97	10.7
		Reverse	0.697	32.78		62.83	10.5

respectively, compared to FF values at +20 °C. Figure 3(d) shows the PCE; remarkably, the PbS-MPA device's PCE improved under low temperatures, even down to −100 °C, due to a low decline in FF and improvement in V_{OC}. The change in PbS-MPA CQDSCs device under low temperatures is similar to reported by Speirs *et al.*[20] The PCE of P3HT, and PBDB-T devices dropped up to 18% and 65% at −100 °C, respectively. Under high temperatures, PBDB-T devices performed better than PbS-MPA and P3HT, dropped only 5% at 80 °C. However, PbS-MPA devices show a drop in PCE at high temperatures and declined up to 22% at +80 °C. PBDB-T is an organic semiconductor; its low crystallinity in nature impacts the charge carrier transport phenomenon, and it is dominated by thermally activated hopping.[21] PBDB-T crystallinity gradually increases under high temperature, which results in improving FF [Fig. 3(c)]. P3HT shows stability even up to 150 °C; the decline in performance is due to PTAA as it starts degrading under high temperatures [Fig. 3(d)].[22–24] PbS QDs have shown stable performance under low temperatures.[20,25] Overall, PbS-MPA and P3HT devices maintain their PCE than PBDB-T devices under HAPS environment. Moreover, PbS-MPA devices can be attractive for operation at low temperatures.

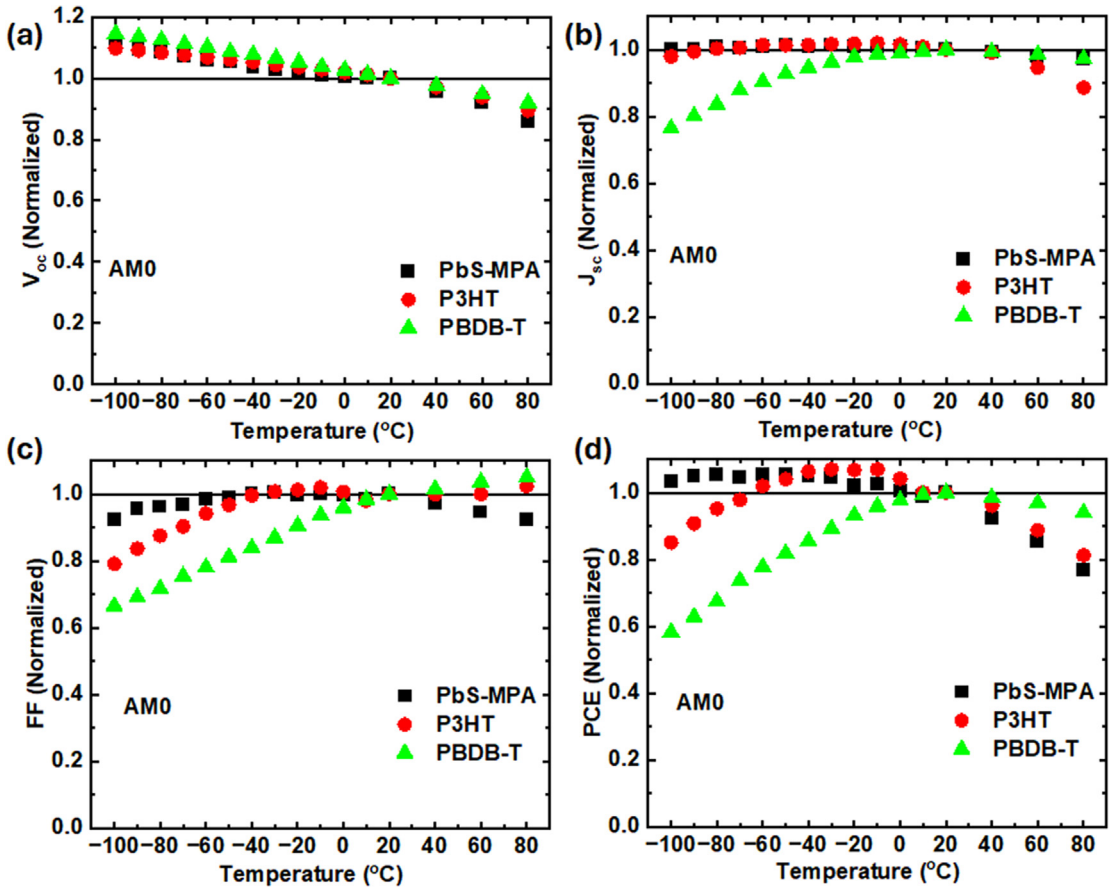

FIG. 3. Normalized (a) V_{OC}, (b) J_{SC}, (c) FF, and (d) PCE of PbS-MPA, P3HT, and PBDB-T CQDSCs devices measured at different temperatures varied from +80 to −100 °C. The black line is drawn at the y axis to guide the reader to follow the normalized value at 1.

Figure 4 shows normalized thermal cycling stability data for PbS-MPA, P3HT, and PBDB-T CQDSCs. The study was conducted by cycling temperature at the rate of 30 °C/min from +20 °C and down to −85 °C, considering the temperature variation in the HAPS environment over a day–night. In total, 16 cycles were recorded, and the devices were measured under AM0 irradiation after the temperature reached at +20 °C. V_{OC} was stable for PbS-MPA, and there was a bit decline in V_{OC} for P3HT and PBDB-T, as shown in Fig. 4(a). However, J_{SC} [Fig. 4(b)] was stable for PbS-MPA and P3HT devices, whereas PBDB-T device's J_{SC} started declining after the eighth cycle and dropped by 10% at the end of 16th cycle. FF [Fig. 4(c)] also shows a similar impact, stable for PbS-MPA and P3HT and dropped for PBDB-T devices with increasing cycles. For the PCE, the PbS-MPA device has no drop in the performance [Fig. 4(d)] over all 16 cycles. P3HT device shows a slight drop in PCE, whereas PBDB-T devices showed ∼20% drop in PCE at the 16th cycle. PbS-MPA devices are entirely inorganic and may not suffer from the degradation pathways that affect organic semiconductors (P3HT and PBDB-T) under thermal cycling.[20,26,27]

In this work, the PbS-MPA colloidal quantum dots-based solar cells were explored under the HAPS environment. Three devices were included using three different types of hole transport layer combinations named PbS-MPA, P3HT, and PBDB-T. The study included low-temperature and thermal cycling stability measurements under AM0 irradiation. The devices delivered PCE (at 20 °C, under AM0) of 8.41%, 7.86%, and 10.77% for PbS-MPA, P3HT, and PBDB-T devices, respectively. Under HAPS operating temperature (+10 to −20 °C), PCE was improved for PbS-MPA and P3HT devices, whereas it decreased for PBDB-T devices. Interestingly, at −100 °C, the PCE of the PbS-MPA devices enhanced 3.5%. Meanwhile, for P3HT and PBDB-T devices, PCE dropped by 15% and 42 %, respectively, under similar conditions. PCE of PbS-MPA devices improved at low temperatures, which shows its ability for applications beyond HAPS environments. PbS-MPA devices also show excellent thermal cycling stability and maintain 100% of PCE even after completing 16 cycles. In summary, this study indicates the role of hole transport layer selection and shows that the PbS-MPA CQDSCs can be feasible for HAPS application. Furthermore, PbS-MPA devices have attractive potential for working beyond the HAPS region.

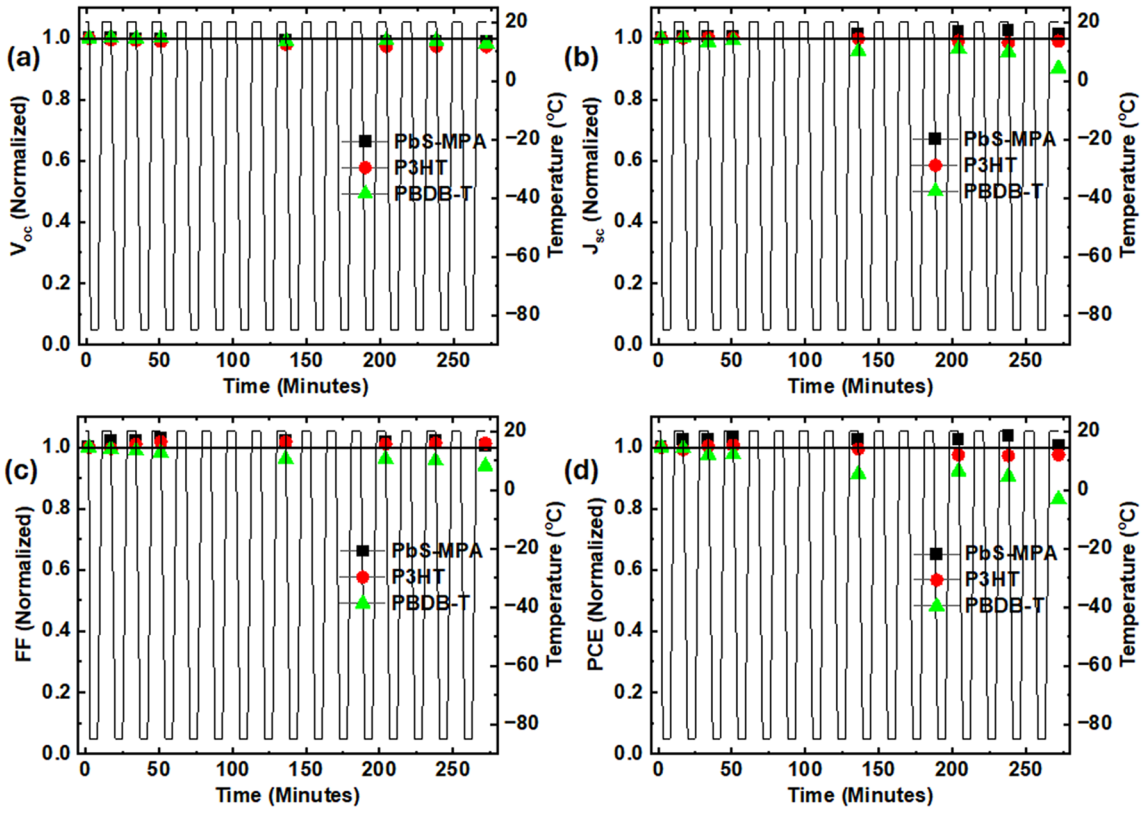

FIG. 4. Normalized (a) V_{OC}, (b) J_{SC}, (c) FF, and (d) PCE of PbS-MPA, P3HT, and PBDB-T devices thermal cycling (+20 to −85 °C) data measured under AM0. The black line is drawn at the y-axis to guide the reader to follow the normalized value at 1.

See the supplementary material for the device fabrication procedure, supporting data tables, and J-V characteristics measured using both scans (forward and reverse), including JV characteristics measured at different temperatures and thermal cycling.

R.D. and W.C.T. sincerely acknowledges the ATIP (EP/T028513/1) grant for providing financial support. Z.L. acknowledges the National Natural Science Foundation of China (Grant No. 52372215) grant for providing financial support.

AUTHOR DECLARATIONS

Conflict of Interest

The authors have no conflicts to disclose.

Author Contributions

Ram Datt: Conceptualization (lead); Data curation (equal); Formal analysis (lead); Investigation (lead); Methodology (lead); Resources (lead); Writing – original draft (lead); Writing – review & editing (lead). **Xin Wen:** Formal analysis (equal); Investigation (equal); Resources (equal); Visualization (equal); Writing – original draft (equal); Writing – review & editing (equal). **Xiaobo Ding:** Formal analysis (equal); Resources (equal); Writing – original draft (equal); Writing – review & editing (equal). **Zeke Liu:** Conceptualization (equal); Formal analysis (equal); Funding acquisition (equal); Project administration (equal); Supervision (equal); Writing – review & editing (equal). **Wanli Ma:** Conceptualization (supporting); Funding acquisition (supporting); Project administration (supporting); Resources (supporting). **Wing Chung Tsoi:** Conceptualization (equal); Funding acquisition (equal); Investigation (equal); Project administration (equal); Resources (equal); Supervision (equal); Writing – review & editing (equal).

DATA AVAILABILITY

The data that support the findings of the study are available in this manuscript and in the supplementary material.

REFERENCES

[1]M. A. Cotta, "Quantum dots and their applications: What lies ahead?," ACS Appl. Nano Mater. **3**(6), 4920–4924 (2020).
[2]X. Gong, Z. Yang, G. Walters, R. Comin, Z. Ning, E. Beauregard, V. Adinolfi, O. Voznyy, and E. H. Sargent, "Highly efficient quantum dot near-infrared light-emitting diodes," Nat. Photonics **10**(4), 253–257 (2016).
[3]S. Ghosh, S. Hoogland, V. Sukhovatkin, L. Levina, and E. H. Sargent, "A tunable colloidal quantum dot photo field-effect transistor," Appl. Phys. Lett. **99**(10), 101102 (2011).

[4]H. C. Liu, M. Gao, J. McCaffrey, Z. R. Wasilewski, and S. Fafard, "Quantum dot infrared photodetectors," Appl. Phys. Lett. **78**(1), 79–81 (2001).
[5]I. J. Kramer, G. Moreno-Bautista, J. C. Minor, D. Kopilovic, and E. H. Sargent, "Colloidal quantum dot solar cells on curved and flexible substrates," Appl. Phys. Lett. **105**(16), 163902 (2014).
[6]Y. Liu, Y. Gao, Q. Yang, G. Xu, X. Zhou, G. Shi, X. Lyu, H. Wu, J. Liu, S. Fang, M. I. Ullah, L. Song, K. Lu, M. Cao, Q. Zhang, T. Li, J. Xu, S. Wang, Z. Liu, and W. Ma, "Breaking the size limitation of directly-synthesized PbS quantum dot inks toward efficient short-wavelength infrared optoelectronic applications," Angew. Chem., Int. Ed. **62**(17), e202300396 (2023).
[7]N. Sukharevska, D. Bederak, V. M. Goossens, J. Momand, H. Duim, D. N. Dirin, M. V. Kovalenko, B. J. Kooi, and M. A. Loi, "Scalable PbS quantum dot solar cell production by blade coating from stable inks," ACS Appl. Mater. Interfaces **13**(4), 5195–5207 (2021).
[8]X. Ding, X. Wen, Y. Kawata, Y. Liu, G. Shi, R. ben Ghazi, X. Sun, Y. Zhu, H. Wu, H. Gao, Q. Shen, Z. Liu, and W. Ma, "*In situ* synergistic halogen passivation of semiconducting PbS quantum dot inks for efficient photovoltaics," Nanoscale **16**(10), 5115–5122 (2024).
[9]J. Li, X. Zhang, Z. Liu, H. Wu, A. Wang, Z. Luo, J. Wang, W. Dong, C. Wang, S. Wen, Q. Dong, W. W. Yu, and W. Zheng, "Optimizing energy levels and improving film compactness in PbS quantum dot solar cells by silver doping," Small **20**(29), 2311461 (2024).
[10]Y. Wang, H. Wu, H. Gao, Q. Ren, K. Ni, S. Liu, W. Ma, J. Wang, Z. Liu, and R. Liu, "Hybrid thin film encapsulation for improving the stability of PbS quantum dot solar cells," Small **20**(45), 2404984 (2024).
[11]S. Zheng, X. Mei, J. Chen, E. M. J. Johansson, and X. Zhang, "Colloidal quantum dot for infrared-absorbing solar cells: State-of-the-art and prospects," Nano Res. Energy **3**(1), e9120095 (2024).
[12]G. H. Carey, A. L. Abdelhady, Z. Ning, S. M. Thon, O. M. Bakr, and E. H. Sargent, "Colloidal quantum dot solar cells," Chem. Rev. **115**(23), 12732–12763 (2015).
[13]C. Ding, D. Wang, D. Liu, H. Li, Y. Li, S. Hayase, T. Sogabe, T. Masuda, Y. Zhou, Y. Yao, Z. Zou, R. Wang, and Q. Shen, "Over 15% efficiency PbS quantum-dot solar cells by synergistic effects of three interface engineering: Reducing nonradiative recombination and balancing charge carrier extraction," Adv. Energy Mater. **12**(35), 2201676 (2022).
[14]R. Datt, H. K. H. Lee, G. Zhang, H. Yip, and W. C. Tsoi, "Organic solar cells at stratospheric condition for high altitude platform station application," Chin. J. Chem. **40**(24), 2927–2932 (2022).
[15]S. Bauk, "Performances of some autonomous assets in maritime missions," TransNav **14**(4), 875–881 (2020).
[16]J. Barbé, A. Pockett, V. Stoichkov, D. Hughes, H. K. H. Lee, M. Carnie, T. Watson, and W. C. Tsoi, "*In situ* investigation of perovskite solar cells' efficiency and stability in a mimic stratospheric environment for high-altitude pseudo-satellites," J. Mater. Chem. C **8**(5), 1715–1721 (2020).
[17]X. Zhang, V. A. Öberg, J. Du, J. Liu, and E. M. J. Johansson, "Extremely lightweight and ultra-flexible infrared light-converting quantum dot solar cells with high power-per-weight output using a solution-processed bending durable silver nanowire-based electrode," Energy Environ. Sci. **11**(2), 354–364 (2018).
[18]M. M. Tavakoli, M. H. Gharahcheshmeh, N. Moody, M. G. Bawendi, K. K. Gleason, and J. Kong, "Efficient, flexible, and ultra-lightweight inverted PbS quantum dots solar cells on all-CVD-growth of parylene/graphene/oCVD PEDOT substrate with high power-per-weight," Adv. Mater. Interfaces **7**(16), 2000498 (2020).
[19]R. Verduci, V. Romano, G. Brunetti, N. Yaghoobi Nia, A. Di Carlo, G. D'Angelo, and C. Ciminelli, "Solar energy in space applications: Review and technology perspectives," Adv. Energy Mater. **12**(29), 2200125 (2022).
[20]M. J. Speirs, D. N. Dirin, M. Abdu-Aguye, D. M. Balazs, M. V. Kovalenko, and M. A. Loi, "Temperature dependent behaviour of lead sulfide quantum dot solar cells and films," Energy Environ. Sci. **9**(9), 2916–2924 (2016).
[21]J. Liu, Y. Yin, K. Wang, P. Wei, H. Lu, C. Song, Q. Liang, and W. Huang, "Domain size control in all-polymer solar cells," iScience **25**(4), 104090 (2022).
[22]F. M. Rombach, S. A. Haque, and T. J. Macdonald, "Lessons learned from spiro-OMeTAD and PTAA in perovskite solar cells," Energy Environ. Sci. **14**(10), 5161–5190 (2021).
[23]A. Rodrigues, M. C. R. Castro, A. S. F. Farinha, M. Oliveira, J. P. C. Tomé, A. V. Machado, M. M. M. Raposo, L. Hilliou, and G. Bernardo, "Thermal stability of P3HT and P3HT:PCBM blends in the molten state," Polym. Test. **32**(7), 1192–1201 (2013).
[24]S. Brixi, O. A. Melville, N. T. Boileau, and B. H. Lessard, "The influence of air and temperature on the performance of PBDB-T and P3HT in organic thin film transistors," J. Mater. Chem. C **6**(44), 11972–11979 (2018).
[25]C. Cheng, J. Li, and X. Cheng, "Photoluminescence lifetime and absorption spectrum of PbS nanocrystal quantum dots," J. Lumin. **188**, 252–257 (2017).
[26]V. Coropceanu, J. Cornil, D. A. da Silva Filho, Y. Olivier, R. Silbey, and J. L. Brédas, "Charge transport in organic semiconductors," Chem. Rev. **107**(4), 926–952 (2007).
[27]H. Li, C. Li, L. Duan, and Y. Qiu, "Charge transport in amorphous organic semiconductors: Effects of disorder, carrier density, traps, and scatters," Isr. J. Chem. **54**(7), 918–926 (2014).